

# Vapor-Phase CMAS-Induced Degradation of Adhesion of Thermal Barrier Coatings

Vladimir Tolpygo<sup>1</sup> 

Received: 26 November 2016 / Published online: 24 January 2017  
© Springer Science+Business Media New York 2017

**Abstract** An investigation of the interface degradation and failure of EB-PVD thermal barrier coatings (TBCs) during burner rig cyclic oxidation in the presence of calcium–magnesium–alumino-silicate (CMAS) deposits has been conducted. The formation of two compounds of major CMAS constituents, specifically  $MgAl_2O_4$  (spinel) and  $CaAl_2Si_2O_8$  (anorthite), was observed at the interface between the alumina scale and the TBC. Spallation occurred as a result of cracking and delamination primarily through the spinel layer. The tests showed more than a tenfold decrease in TBC life relative to the oxidation test without CMAS at the same temperature. It is demonstrated that this particular form of coating degradation occurs below the melting temperature of this particular CMAS composition and hence does not involve TBC infiltration by molten silicates. The likely mechanism of interface degradation, which involves vapor-phase transport of CMAS constituents as hydroxides, is proposed and discussed.

**Keywords** Thermal barrier coatings (TBCs) · Calcium magnesium alumino-silicate (CMAS) · Alumina scale · Adhesion

## Introduction

This work describes the role of calcium–magnesium–alumino-silicate (CMAS) in spallation failure of thermal barrier coatings (TBCs) that are used to protect hot section components of gas turbines. Silica-rich particles are ingested during engine operation in dusty environments. The interaction of molten silicates with TBCs has been a subject of extensive research over the past decades [1]. It is commonly accepted that the major form of TBC degradation by CMAS is liquid-phase

---

✉ Vladimir Tolpygo  
vladimir.tolpygo@honeywell.com

<sup>1</sup> Honeywell Aerospace, 111 S. 34th St., M/S 503-118, Phoenix, AZ 85034, USA

infiltration into the TBC that causes a reduction in strain compliance (stiffening) of the coating and an increase in thermal stresses during cooling. This mechanism is particularly relevant to the EB-PVD TBCs, which have a network of open channels in the form of inter-columnar gaps spanning through the whole thickness of the coating. In this case, CMAS infiltration is driven by capillarity and its penetration depth depends on temperature, time, chemical composition and viscosity. Correspondingly, the common premise is that CMAS resides on TBC surface as viscous glass, so if the surface temperature is lower than the melting or glass transition temperature, the problem should not be relevant.

However, there exists another CMAS degradation mechanism, described in this paper, which remains virtually unknown in the published literature. The damage occurs primarily at the interface between the TBC and the thermally grown oxide (TGO) that forms on the bond coat surface. Most importantly, this mechanism does not involve molten silicates so the transport of their constituents toward the TGO presumably occurs through the vapor phase. It may be argued that fine dust particles ingested into the hot section of a modern gas turbine should volatilize in the combustor and form various hydroxides in the presence of water vapor in the combustion environment. So the coatings on airfoils interact with combustion products enriched with vapor-phase CMAS, rather than liquid droplets or solid particles.

Depending on the TBC temperature and CMAS composition, these hydroxides may condense to form a molten or solid deposit on the surface, but they can also permeate through the open porosity in the coating. This paper is focused on microstructural evidence of CMAS attack of the TGO-YSZ interface leading to a drastic reduction in TBC life during burner rig testing. It is demonstrated that CMAS constituents form layers of spinel and anorthite at the alumina–YSZ interface that cause delamination of the coating. Experimental verification of the proposed mechanism is a subject of a separate publication [2].

## Experimental Procedures

In this work, CMAS-induced degradation of the standard EB-PVD 7YSZ (7 wt% yttria-stabilized zirconia) TBC, about 150 microns thick, with a platinum-modified aluminide bond coat was investigated. The coating was deposited on 4" long and 0.5" diameter bars of SC180 second-generation superalloy. Cyclic oxidation tests were conducted at 1150 °C with 30 min dwell per cycle using a burner rig. The burner operated on a mixture of jet fuel with compressed air. The bars were positioned normal to the flame direction on a carousel holder rotating at 800 RPM to achieve similar temperature distributions for a group of 8 bars tested simultaneously. The temperature was controlled by two Pt/Pt–Rh thermocouples inserted into axial holes in the bars. The ramp rate was calibrated to prevent significant temperature gradients between TBC surface and the thermocouple. The target temperature was maintained over a 20–25 mm-long "hot zone" in the middle of the bars with variations not exceeding  $\pm 10$  °C. In this experimental setup, the TBC surface and the TBC-bond coat interface are at the same temperature during each

30 min segment. The tests were typically conducted until TBC spallation, but some specimens were removed from the rig prior to failure for sectioning and analysis of TBC and TGO microstructure (Table 1).

The selection of CMAS composition was based on chemical analysis of ingested sand collected on test engine parts after operation on the ground level in Arizona desert. Five principal oxide constituents were formulated in the following proportion:  $15\text{CaO}-12\text{MgO}-8\text{FeO}_{1.5}-20\text{AlO}_{1.5}-45\text{SiO}_2$  (in mole percent for single cation formulae), hereafter abbreviated as CMFAS. In order to avoid erosion damage of TBC by solid particulate during the test, an aqueous solution of the corresponding nitrates mixed with colloidal silica was prepared and injected directly into the burner, as proposed in Ref. [3]. The concentration of constituents corresponded to the total of 1 wt% of all oxides. The solution was dispensed through an “atomizer” at 1 ml/min producing 20–30 mg of solid deposit on the hot section of each bar after one 30 min cycle.

It is quite obvious that the solution instantly evaporates inside the burner; therefore, the CMFAS should be present in the flame as various vapor species, presumably in the form of hydroxides. Preliminary analysis of the selected composition by DSC has shown that its melting temperature is approximately 1220 °C, which is 70 °C higher than the test temperature used in this work. For this reason, the vapor phase may be expected to condense into small particles and adhere to the TBC surface at 1150 °C. Indeed, Fig. 1 demonstrates typical morphology of the deposit, which consists of loosely attached particles, rather than a glassy phase typical of molten silicates. This indicates that the selected CMFAS composition is present on TBC surface primarily as solid deposit in the course of testing. A small amount of liquid phase may still be possible due to local chemistry variations.

Analysis of CMFAS composition by EDX on cross sections, such as in Fig. 1c, shows somewhat different proportion of the oxides, which can be described as  $20\text{CaO}-10\text{MgO}-8\text{FeO}_{1.5}-22\text{AlO}_{1.5}-40\text{SiO}_2$  with minor additions of NaO (an

**Table 1** Nominal chemical composition of SC180 superalloy (weight percent)

Cr	Co	Mo	W	Ta	Ti	Al	Re	Hf	Ni
5.0	10.0	2.0	5.0	8.5	1.0	5.2	3.0	0.1	Bal.

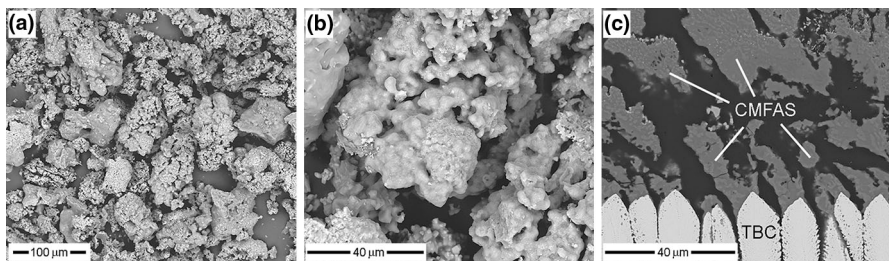


**Fig. 1** Morphology of CMFAS deposit indicating the absence of molten phase during testing at 1150 °C: lower (a) and higher magnification (b) SEM images; polished section of CMFAS on TBC surface (c)

impurity in colloidal silica). The reduced concentration of silica in the deposit relative to the initial composition may be due to higher equilibrium pressure of silicon hydroxide [2] or, more likely, due to the difference in condensation kinetics of various species. Based on the BSE image contrast, the condensed CMFAS consists of several different phases; however, their analysis is beyond the scope of this work.

## Results and Discussion

All the tests with CMFAS-enriched flame resulted in TBC spallation after less than 100 cycles, (<50 h at 1150 °C), which is less than a tenth of the average spallation life of this TBC system during regular burner rig oxidation at the same temperature. Analysis of spalled pieces (Fig. 2) indicates that stiffening of the coating is not a factor in TBC failure. The columns are still separated by inter-columnar gaps that are not filled with glassy phase, so strain compliance was probably not significantly affected by CMFAS. The higher magnification images in Fig. 2 show distinct feathery morphology of YSZ columns and individual precipitates attached to the columns. The concentration of major elements, measured by EDX, indicates that these particles can be identified as  $\text{CaAl}_2\text{Si}_2\text{O}_8$  (anorthite). In some cases, inclusions of zirconium silicate,  $\text{ZrSiO}_4$ , can also be found.

Another illustration of TBC morphology after CMFAS testing is shown in Fig. 3. This coating has been mounted in epoxy and polished at a small angle to the surface in order to expose the top view at different spans through TBC thickness. The taper section image and elemental maps confirm the presence of wide open gaps between YSZ columns (the map of carbon is included to demonstrate TBC infiltration by epoxy), with many anorthite particles around the columns. Interestingly, very little magnesium and iron can be found in the TBC interior, whereas both elements are present on the TBC surface. With no sign of CMFAS melt infiltration, the likely mechanism of anorthite formation is condensation of calcia, alumina and silica from the vapor phase.

Further analysis of the spalled TBC reveals the presence of about 5- $\mu\text{m}$ -thick layer at the bottom of the coating, where an alumina TGO might be expected.

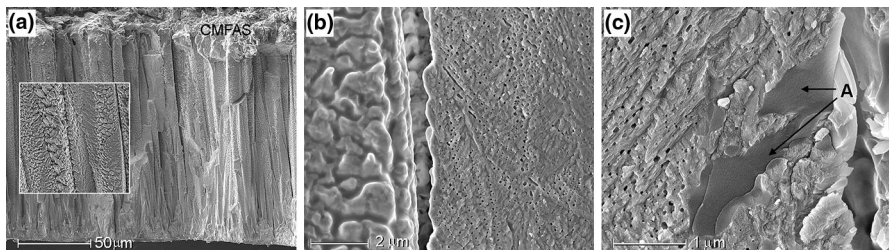


**Fig. 2** Microstructure of spalled TBC after CMFAS testing for 60 cycles at 1150 °C: **a** general view; **b** higher magnification showing fracture section through YSZ column and *open gap* between columns; **c** anorthite inclusion (marked A) attached to the column surface

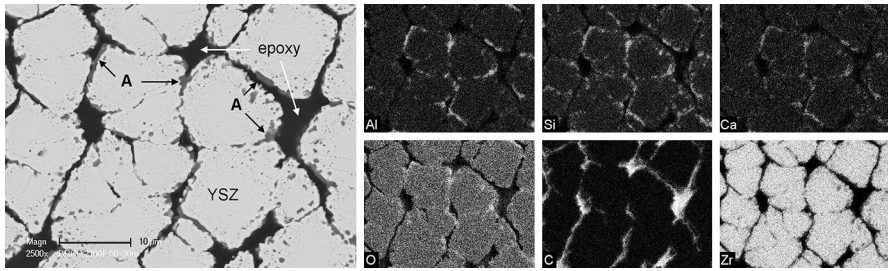


**Fig. 3** TBC taper section (BSE mode) after CMFAS testing for 50 cycles at 1150 °C and EDX maps of selected elements, showing *open gap* between columns (infiltrated with epoxy) and individual precipitates of anorthite (A) around TBC columns

However, this layer consists of anorthite and spinel, as illustrated in Fig. 4b, whereas the alumina scale remains on the bar surface (not shown here). The flip side of the spalled TBC exposes two types of microstructure. One is highly porous  $MgAl_2O_4$  with some iron and nickel, consisting of sub-micron size crystals, as shown in Fig. 4e. The other is fully dense  $CaAl_2Si_2O_8$  with some Na and Mg, apparently as crystalline phase, based on the appearance of its fracture surface in Fig. 4f. The composition and crystalline structure of both layers have been confirmed by the TEM analysis [2]. The presence of nickel in the spinel layer, illustrated by the EDX spectrum in Fig. 4e, is noteworthy as will be discussed later. Hence, TBC failure occurs neither at the TBC-TGO interface, nor at the TGO-bond coat interface, as might be expected during regular oxidation tests, but rather through the layers of CMFAS oxides that develop between alumina and TBC.

In some instances, the exact location of the delamination crack can be found, as shown in Fig. 5. In this case, a large separation, about 3 mm wide, develops prior to

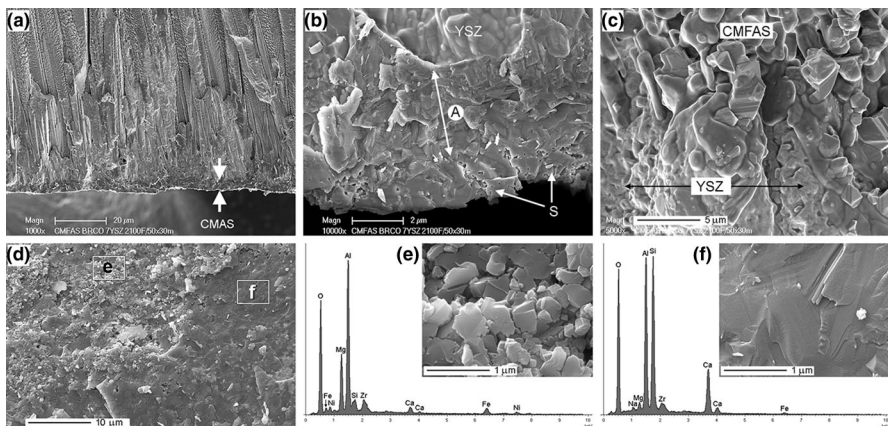


**Fig. 4** Microstructure of spalled TBC after 50 cycles at 1150 °C: **a** general view showing a layer marked CMAS at the *bottom* of TBC; **b** higher magnification view of the layer (A anorthite, S spinel); **c** CMFAS deposit on TBC *top* surface; **d** underside of the spalled TBC exposing fracture surface with *rectangular boxes* of higher magnification images in **e** and **f** with corresponding EDX spectra of the selected areas

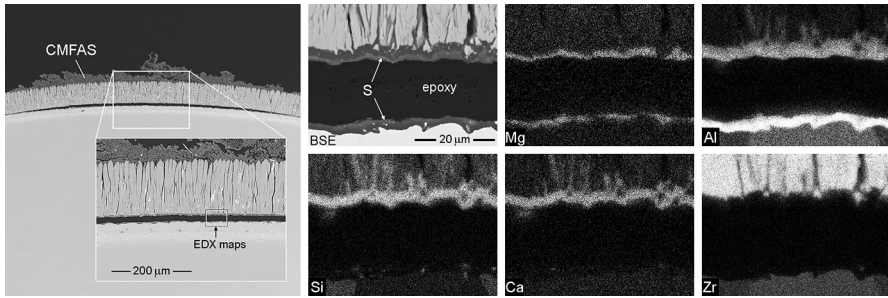


**Fig. 5** Cross section showing TBC buckling as a result of delamination through the spinel layer ( $S \text{ MgAl}_2\text{O}_4$ ). Note the presence of Mg and Al on both side of the crack

TBC spallation. This separation is a typical example of buckling failure as a result of thermal mismatch stress in the coating. The cross section and elemental distributions in Fig. 5 show that delamination occurs through the spinel layer, as illustrated by the Mg map, whereas the alumina scale remains fully adherent to the bond coat. The maps of silicon and calcium indicate location of the anorthite layer directly above the spinel.

Another example of TBC failure is shown in Fig. 6. The higher magnification images of the interface in the vicinity of the spalled section confirm that delamination crack propagates above the TGO through the spinel layer. Apparently, the porous structure of  $\text{MgAl}_2\text{O}_4$  (Fig. 4e) is susceptible to cracking under thermal stresses, so the spinel layer becomes a “weak link” in the whole TBC system. The fact that the crack also propagates through the anorthite layer (Fig. 4d) and occasionally across YSZ (Fig. 6c) simply means that the fracture path does not follow all interface undulations.

It is important to point out that the alumina scale thickness in Fig. 6c is about  $2 \mu\text{m}$ , which is 3–4 times smaller than the critical TGO thickness upon TBC spallation during oxidation tests of similar systems without CMAS. It is clear that the CTE mismatch stress in alumina does not play a role in TBC spallation, since the scale remains adherent. Hence, the driving force for delamination is the stress in the TBC and especially in the dense layer of anorthite, which has thermal expansion coefficient ( $4.8 \times 10^{-6} \text{ C}^{-1}$  [4]) almost twice lower than alumina and spinel.

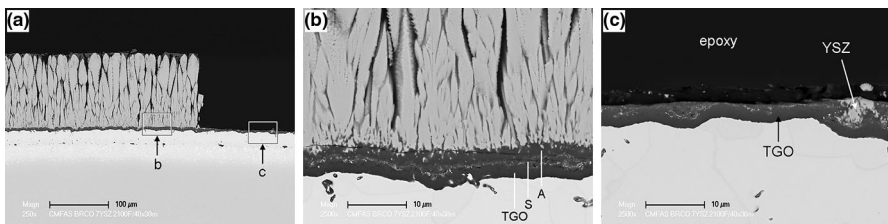


**Fig. 6** TBC spallation after 40 cycles at  $1150 \text{ }^\circ\text{C}$ : **a** general view with *rectangular boxes* corresponding to higher magnification images in **b** and **c**. The three-layer structure at the TBC-bond coat interface is shown in **b**: TGO— $\text{Al}_2\text{O}_3$ ; S— $\text{MgAl}_2\text{O}_4$ ; A— $\text{CaAl}_2\text{Si}_2\text{O}_8$

Observations of the three-layer structure that develops between the TBC and the bond coat during burner rig testing in the presence of CMFAS did not provide sufficient data to establish the growth kinetics of all three layers. The principal difficulty was that the formation of spinel and anorthite was not uniform over the perimeter of the bars. It appears that permeation of vapor species through TBC depends on the position relative to the flame and direction of the gas flow. For this reason, condensation at the TGO-YSZ interface is more pronounced in some areas and less in the others. Nevertheless, the microstructures after various exposure times (Fig. 7) indicate that both spinel and anorthite layers thicken with time.

Several key features of the microstructures in Fig. 7 should be noted. First is the presence of fine particles in the mid-section of the spinel layer. These are precipitates of  $\text{HfO}_2$  and  $\text{ZrO}_2$  (with some yttrium). The hafnium oxide forms as a result of outward diffusion from the Hf-doped bond coat through the scale. In the absence of CMFAS, these particles would be located at the alumina–YSZ interface, but in the current conditions they are dispersed in the spinel layer. This may be an indication that spinel is growing inward and consuming the outer layer of  $\text{Al}_2\text{O}_3$  with  $\text{HfO}_2$  inclusions. The small amount of nickel in the spinel, noted in Fig. 4e, is also a sign that  $\text{MgAl}_2\text{O}_4$  incorporates a portion of the alumina TGO, which commonly has a small amount of nickel oxides at the outer surface.

The presence of zirconia particles shows the initial location of the TGO-YSZ interface, which is now inside the spinel layer. Some zirconia inclusions are also dispersed inside the anorthite layer. Because of the small size of these particles and overlapping signals of yttrium and zirconium, it was not possible to determine the exact amount of yttrium using SEM/EDX. However, there are indications that yttrium concentration is significantly higher than in the original 7YSZ, which means that there is partial dissolution of zirconia in the anorthite layer. Since no liquid phase is involved, this must be a result of solid-state reaction and diffusion between  $\text{ZrO}_2$  and  $\text{CaAl}_2\text{Si}_2\text{O}_8$ .

The fact that the  $\text{MgAl}_2\text{O}_4$  layer thickens with time is a clear sign that magnesium diffuses through the dense  $\text{CaAl}_2\text{Si}_2\text{O}_8$  layer and reacts with alumina TGO. Correspondingly, condensation of magnesium hydroxide continues on top of the anorthite. It is not clear whether the source of aluminum, present in the  $\text{MgAl}_2\text{O}_4$  layer, is solely from the alumina scale or from the aluminum hydroxide vapor (or both). The amount of iron in the spinel (1–2%, Fig. 4e) is much smaller

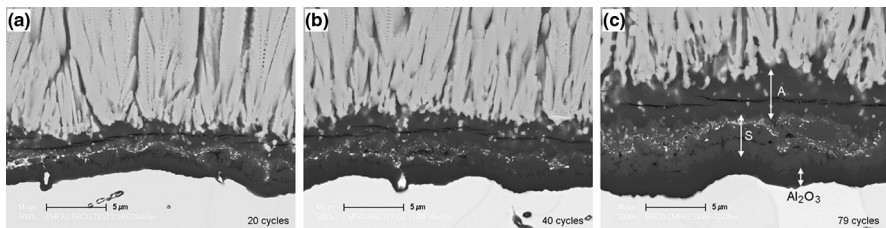


**Fig. 7** Typical microstructures of CMFAS build-up at the interface between alumina TGO and TBC after 20 (a), 40 (b) and 79 cycles (S spinel, A anorthite). All images are taken at the same magnification. The bright precipitates in the scale are hafnia and zirconia

than in the original CMFAS (8%), so its vapor transport is much reduced relative to the other CMFAS constituents. The growth of anorthite is particularly interesting. The layer is fully dense (Fig. 4f) and remains in direct contact with YSZ with virtually no pores or separations between  $\text{CaAl}_2\text{Si}_2\text{O}_8$  and zirconia. Apparently, this layer gradually pushes TBC away from the TGO, and any open spaces that may develop get filled with new condensate. This is quite different from the condensation process in the interior of the TBC (Figs. 2, 3) where anorthite particles are present as individual inclusions rather than a continuous layer. It may be speculated that preferential condensation at the TGO-YSZ interface is related to the impingement of the gas flowing along the inter-columnar gaps inwards. Note that the top surface deposit remains discontinuous (Fig. 1c), so there is sufficient gas passage through the TBC.

The cracks in the anorthite layer, seen in all images in Fig. 7, are likely a result of sectioning and polishing, which is not surprising because this layer is expected to be under very high compressive stress due to the thermal expansion mismatch between the superalloy and  $\text{CaAl}_2\text{Si}_2\text{O}_8$ . The actual delamination crack usually propagates through the porous spinel layer below, as demonstrated earlier. Note that there is almost no difference in thickness of the alumina scale between 10 h of exposure (Fig. 7a) and 39.5 h (Fig. 7c). In both cases, the scale is about 1.5  $\mu\text{m}$  thick, which confirms the hypothesis that the spinel layer consumes a portion of the alumina TGO. The combined thickness of the other two layers in Fig. 7(c) created as a result of CMFAS exposure is about 7 microns. For comparison, the scale thickness for the same TBC system without CMFAS is approximately 3  $\mu\text{m}$  after 79 30 min cycles at 1150 °C.

The cross section in Fig. 8 shows the microstructure and distribution of several major elements in the three-layer structure that develops between the bond coat and the TBC after 79 cycles at 1150 °C away from the failure site. A thick layer (4–5  $\mu\text{m}$ ) of spinel is illustrated by the map of magnesium, whereas the maps of silicon and calcium show the location of the anorthite layer above. It is important to note that the gaps between YSZ columns are also filled with anorthite in the bottom portion of the TBC. This feature becomes more distinct near the end of TBC life in the current CMFAS tests. Unlike the mid-span TBC sections that retain strain compliance (Fig. 3), the bottom layer adjacent to anorthite is almost fully dense.

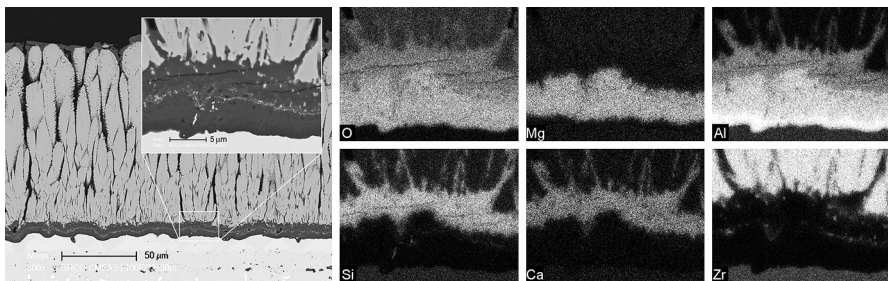


**Fig. 8** TBC-polished cross section 79 cycles CMFAS testing at 1150 °C. The EDX maps of selected elements illustrate distribution of major constituents in the higher magnification *inset*



Certainly, the absence of open inter-columnar gaps in the coating should contribute to the driving force for spallation. In other words, in addition to the elastic strain energy in the dense  $\text{CaAl}_2\text{Si}_2\text{O}_8$  layer, increased stiffness of the anorthite-filled YSZ is expected to drive TBC spallation, similar to the effect of liquid-phase infiltration [5]. As opposed to common cyclic oxidation conditions when TBC spallation occurs at the TGO–bond coat interface, the current multi-layer structure includes a porous spinel layer. This factor explains poor TBC adhesion and short cyclic lives in the presence of CMFAS.

Finally, it is instructive to compare the CMFAS reaction with the TGO, examined during the burner rig tests, with one example of TGO degradation observed on TBC coated airfoils after engine operation in a dusty environment. Some areas on the pressure side of the airfoils exhibited TBC spallation. The cross section (away from the failure site) in Fig. 9 demonstrates similar build-up of spinel and anorthite on top of alumina TGO, whereas the inter-columnar gaps in the mid-span of the TBC are not filled by CMAS. The layers also incorporate small inclusions of zirconia, similar to the microstructures in Figs. 7 and 8. One notable difference from the burner rig results is that on the airfoil a distinct string of small pores developed between the spinel layer and alumina. It is visible on the high magnification insert, as well as oxygen and aluminum maps in Fig. 9. Microstructural analysis in the vicinity of spalled areas confirms that delamination occurs along the string of pores, i.e., at the alumina–spinel interface rather than through the spinel layer as in the laboratory tests.

Recently, a vapor-phase mechanism of TBC infiltration has been proposed by Braue [6]. In that case, the presence of calcium sulfate has been observed across the whole TBC cross section on an engine airfoil. The rationale for  $\text{CaSO}_4$  infiltration via vapor phase is rather similar to the present investigation. Since the melting temperature of calcium sulfate (1460 °C) is significantly higher than the TBC surface temperatures, the only plausible infiltration mechanism is through the vapor phase followed by crystallization inside the TBC inter-columnar gaps. Interestingly,

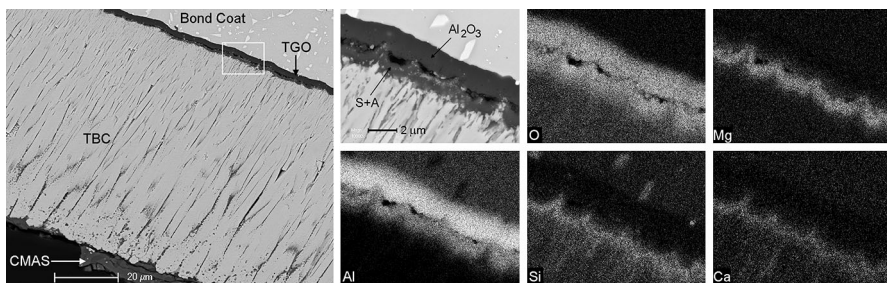


**Fig. 9** TBC cross section on a high-pressure turbine blade after engine operation in CMAS-containing environment. The EDX maps of selected elements illustrate distribution of major CMAS constituents at higher magnification in the area outlined by the *rectangular box*. The alumina TGO and two-layer structure with spinel (S) and anorthite (A) are marked (the bond coat is at the *upper side* of the images). Note that silicon map also shows tantalum-rich gamma-prime grains in the bond coat as a result of overlap between Si and Ta peaks

deposition of  $\text{CaSO}_4$  did not cause TBC decohesion [6], unlike the present experiments and observations.

## Conclusions

A new form of CMAS-induced degradation of thermal barrier coatings is described. It involves infiltration of the TBC by major CMAS constituents, presumably in the form of volatile hydroxides, and condensation at the TBC-TGO interface. The subsequent solid-state reaction with the TGO leads to the formation of a porous  $\text{MgAl}_2\text{O}_4$  spinel layer that is susceptible to cracking and spallation. An additional layer of  $\text{CaAl}_2\text{Si}_2\text{O}_8$  anorthite forms above the spinel layer. Unlike the more common liquid-phase infiltration by CMAS, the proposed mechanism can operate at temperatures below the melting temperature of CMAS, as long as the atmosphere contains water vapor, which makes it relevant to the combustion environment in gas turbines.

The CMAS-induced degradation of TGO-YSZ adhesion is amplified by the formation of a dense layer of anorthite between the spinel and the top coat, which increases the driving force for TBC spallation due to thermal stresses during cyclic exposure. Burner rig tests demonstrated more than a tenfold decrease in TBC spallation life relative to the CMAS-free environment at the same temperature. Further details regarding condensation, crystallization and growth of the detrimental spinel and anorthite layers, which break the bond between alumina and 7YSZ, require a separate investigation.

It should be noted that other CMAS-induced degradation mechanisms, specifically, stiffening of the TBC by melt infiltration and surface reactions that change morphology and phase composition of the coating, are obviously relevant and may be detrimental in different test conditions and with different CMAS chemistries.

**Acknowledgements** This work has been supported by Honeywell Advanced Technology IR&D funds. The assistance of J. Cobb and J. Christopher in burner rig experiments is greatly acknowledged. The author is grateful to Mr. W. Baker (Honeywell) and Prof. C.G. Levi (UCSB) for critical reading of this manuscript.

## References

1. C. G. Levi, J. W. Hutchinson, M. H. Vidal-Sétif, and C. A. Johnson, *MRS Bulletin*, **37**, 932–941 (2012).
2. B. S. Lutz, R. W. Jackson, N. Abdul-Jabbar, V. K. Tolpygo, and C. G. Levi (this conference).
3. T. Steinke, D. Sebold, D. E. Mack, R. Vassen, and D. Stover, *Surface and Coatings Technology* **205**, 2287–2295 (2010).
4. R. A. Gdula, *American Ceramic Society Bulletin* **50**(6), 555 (1971).
5. S. Krämer, S. Faulhaber, M. Chambers, D. R. Clarke, C. G. Levi, J. W. Hutchinson, and A. G. Evans, *Materials Science and Engineering: A* **490**, 26–35 (2008).
6. W. Braue, P. Mechnich, and P. W. M. Peters, *Materials at High Temperatures* **28**(4) 315–323 (2011).